



HAL
open science

A modified stepped frequency phase coding radar waveform designed for the frequency domain algorithm

Mahdi Saleh, Samir-Mohamad Omar, Eric Grivel, Oussama Bazzi

► To cite this version:

Mahdi Saleh, Samir-Mohamad Omar, Eric Grivel, Oussama Bazzi. A modified stepped frequency phase coding radar waveform designed for the frequency domain algorithm. *Digital Signal Processing*, 2019, 88, pp.101-115. hal-02099416

HAL Id: hal-02099416

<https://hal.science/hal-02099416v1>

Submitted on 22 Oct 2021

HAL is a multi-disciplinary open access archive for the deposit and dissemination of scientific research documents, whether they are published or not. The documents may come from teaching and research institutions in France or abroad, or from public or private research centers.

L'archive ouverte pluridisciplinaire **HAL**, est destinée au dépôt et à la diffusion de documents scientifiques de niveau recherche, publiés ou non, émanant des établissements d'enseignement et de recherche français ou étrangers, des laboratoires publics ou privés.



Distributed under a Creative Commons Attribution - NonCommercial 4.0 International License

A Modified Stepped Frequency Phase Coding Radar Waveform Designed for the Frequency Domain Algorithm

Mahdi Saleh^{a,b,*}, Samir-Mohamad Omar^{b,c}, Eric Grivel^a, Oussama Bazzi^b

^a*Bordeaux University - Bordeaux INP ENSEIRB-MATMECA - IMS - UMR CNRS 5218, Talence, FRANCE*
^b*Department of Physics and Electronics, Faculty of Sciences I, Lebanese University, Hadath, Beirut, LEBANON*
^c*CCE Department, School of Engineering, International University of Beirut (BIU), Beirut, Lebanon*

Abstract

A great deal of interest has been paid to enhance the radar range resolution for the last decades. One of the techniques is to construct a waveform combining inter-pulse and intra-pulse modulations. In this paper, stepped frequency (SF) waveform is used to represent the former, whereas phase coding (PC) is considered for the latter. To obtain the high-resolution range profile (HRRP) of a target induced by an SF waveform at the receiver, one of the approaches is the frequency domain (FD) algorithm. It has been successfully applied with SF linear frequency modulation waveforms. However, based on our investigations, processing the SFPC waveform with the FD algorithm does not lead to the performance, in terms of peak sidelobe ratio (PSLR) and integrated sidelobe ratio (ISLR), of the single-carrier phase coding (SCPC) waveform processed with a matched filter (MF). To overcome these drawbacks, we propose to split the spectrum of a phase coded pulse into a predetermined number of portions, and then to successively transmit the time-domain transformed versions of these various portions. The received echoes are then processed with a modified version of the FD algorithm. Our analysis and simulations show that the proposed waveform can be characterized by a PSLR and an ISLR close to those of the SCPC processed with MF in some scenarios.

Keywords: Stepped frequency waveforms, phase coding, intra-pulse modulation, peak sidelobe ratio, FD algorithm.

1. Introduction

During the last decades, a great deal of interest has been paid to high range resolution (HRR) in various radar applications, from synthetic aperture radar (SAR) and ground penetrating radar (GPR) to radar target recognition. The key way to obtain HRR is to select a wide bandwidth waveform. For this purpose, two families can be considered.

On the one hand, waveforms with high instantaneous bandwidths can be used. One of them consists of a train of non-modulated pulses whose durations are of the order of the nanoseconds. Another waveform consists of a train of modulated pulses. In the latter, each pulse is internally modulated in phase or in frequency. This modulation is known as the intra-pulse modulation, and one of its representatives is the linear frequency modulation (LFM). However, the aforementioned waveforms lead to a high sampling rate at the receiver. An expensive analog-to-digital converter (ADC) is hence required.

On the other hand, a waveform that consists of a train of externally modulated pulses can be considered. This

modulation is known as the inter-pulse modulation. The most attractive one is the stepped frequency (SF) waveform [1] [2] [3]. In this waveform, a large bandwidth can be obtained by sequentially changing the carrier frequency equidistantly from one pulse to another in one burst. This makes it possible to reduce the instantaneous bandwidth and hence an ADC with a small sampling rate can be exploited.

In various radar applications, the above two families can be combined. This has the advantage of reducing the number of pulses within the coherent processing interval (CPI)¹. Toward this goal, SF-LFM is considered as one of the most popular waveforms [4] [5] [6] [7] [8] [9]. Nonetheless, two other waveforms, known as stepped-frequency phase coding (SFPC) and SF nonlinear frequency modulation (SF-NLFM), have recently started to attract the attentions of the researchers [10]. In [11], the SFPC waveform was investigated. The range estimation in the presence of moving targets is more precise than that of the SF waveform. Moreover, it was suggested to be used with the through the wall radar (TWR) in order to enhance the anti-radio frequency interference performance [10]. As for the SF-NLFM waveform, Gladkova [12] illustrated its advantage over the SF-LFM waveform in terms of reductions of the

*Corresponding author
Email addresses: mahdi.saleh@u-bordeaux.fr (Mahdi Saleh),
samir.omar@liu.edu.lb (Samir-Mohamad Omar),
eric.grivel@ims-bordeaux.fr (Eric Grivel), obazzi@ul.edu.lb
(Oussama Bazzi)

¹CPI is the amount of time a given target is within the antenna beam on a single scan.

grating-lobe levels.

In most radar systems, the traditional approach to process the received echoes at the receiver consists in applying a matched filter (MF) in one shot to the whole train of the received echoes. The processing of SF waveforms with MF requires a high computational cost. In addition, grating lobes may appear in the high-resolution range profile (HRRP)² [12]. One alternative can be seen as a kind of stretch processing. It includes three different algorithms, namely the IFFT, the time domain (TD), and the frequency domain (FD) algorithms [1]. Concerning the latter, the MF is considered at the level of each received echo separately so that the discrete Fourier transform (DFT) of each received echo is multiplied by the conjugate of the DFT of a reference pulse. Then, an inverse discrete Fourier transform (IDFT) is applied to a concatenated version of the previous results, instead of separately applying it to each individual one. The FD and the IFFT algorithms have computational costs smaller than that of the MF-based approach. However, they have some limitations. The IFFT algorithm produces ghost targets in the HRRP of the extended targets due to the spill-over effect of energy into consecutive coarse range bins [1]. The TD algorithm [13] does not produce ghost targets but suffers from the up-sampling requirement of the narrow-bandwidth pulses prior to the frequency shift. Finally, the FD algorithm can cope with the drawbacks of the TD and the IFFT algorithms, but a DFT must be computed on a relatively large number of samples. Nevertheless, with the recent advances in designing and fabricating powerful processors (FPGAs, DSPs etc.), this no longer constitutes an obstacle for implementing this algorithm in real applications. Whatever the type of algorithm that is considered to detect a single-point target, the range profile usually exhibits one mainlobe and several sidelobes. The levels of the sidelobes with respect to the mainlobe one have a great influence on the probability of detection (PD) and the probability of false alarm (PFA). This can be quantified using two ratios: the peak sidelobe ratio (PSLR) and the integrated sidelobe ratio (ISLR). Various schemes have been proposed to enhance these ratios. In [14], a tapped delay technique is used to suppress the range sidelobes of phase reversal codes. The authors in [15] designed an optimum mismatched filter that can be applied to any phase code. The latter filter reduces the sidelobes at the expense of a slight loss in SNR compared to that obtained from an MF. In a noiseless environment, the PSLR and ISLR that characterize the HRRP obtained by processing a single-carrier phase coding (SCPC) waveform with an MF at the receiver has the same shape as the autocorrelation function of the phase code that is used. However, directly processing an

²HRRP is representative of the reflectivity of the target to an HRR radar waveform projected onto the radar line-of-sight. This 1-D signature characterized by range bins makes it possible to estimate the target size and the positions of some scattering points of the target structure.

SFPC waveform with the FD or the IFFT algorithm leads to a PSLR and an ISLR that are worse than those obtained with an SCPC waveform. The PSLR is limited to -13.2 dB and the ISLR to -9.6 dB.

To overcome these limitations, we propose a modified SFPC waveform derived from the SCPC waveform. Firstly the spectrum of a phase coded pulse is split into a predetermined number of non-overlapping portions. Then, the corresponding time-domain signals are successively transmitted. The latter signals represent the modified SFPC waveform. As this methodology leads to some constraints on selecting the number of portions, two alternative solutions are proposed. The first one consists in splitting the spectrum into non-overlapping portions of different sizes. As for the second, the spectrum is split into overlapping portions of equal size. At the receiver, the processing chain is necessarily modified. The purpose of our analysis is then twofold: firstly, we aim at studying the relevance of the modified waveform compared with the single-carrier phase coding (SCPC) waveform in terms of PSLR, ISLR, and sampling frequency. In addition, the influence of the selected number of portions on the PSLR and the ISLR is investigated. Secondly, we suggest comparing the modified SFPC waveform with the SFPC waveforms processed by either the IFFT or the FD algorithm in terms of PSLR, ISLR, and computational cost.

The remainder of the paper is organized as follows: in section 2, we briefly recall the analytic expressions of the SCPC waveform and various SF waveforms at both the transmitter and the receiver parts. We also present the steps of the FD algorithm to reconstruct the HRRP when an SF-LFM waveform is considered. In addition, some details about the PSLR, the minimum range, and the range resolution are provided. In section 3, the modified SFPC waveform is first presented by focusing on the case of non-overlapping portions and then by dealing with the variants either based on non-overlapping portions or overlapping portions of unequal sizes. Then in section 4, the results of the simulations of the modified SFPC waveform in different scenarios are shown. Finally, conclusions and perspectives are drawn in section 5.

In what follows, note that $*$ denotes the conjugate, $.*$ stands for a multiplication of vectors element by element, and $rect(t)$ stands for a rectangular pulse equal to 1 for $-\frac{1}{2} \leq t \leq \frac{1}{2}$ and zero elsewhere.

2. Waveforms Modeling and FD algorithm

In this section, the SCPC, SF, and SFPC waveforms are presented. Then, the steps of the FD algorithm are briefly recalled. Finally, the definitions of some special radar metrics that are used in the simulation part are given.

2.1. Waveform modeling at the transmitter and the receiver

Let us start with the modeling of the SCPC waveform.

2.1.1. SCPC waveform model

When dealing with phase coding intra-pulse modulation, a pulse with width T_p is modulated by a code sequence of length M . This is done by dividing the pulse into M concatenated sub-pulses of duration T_c , where $T_c = \frac{T_p}{M}$. Each element of the code sequence is represented by a code phase value ϕ_m ($m \in \llbracket 0, M-1 \rrbracket$). Hence, the SCPC waveform is given for $0 \leq t \leq T_p$ by:

$$s_{tx}(t) = \sum_{m=0}^{M-1} A \cdot \text{rect}\left(\frac{t - m \cdot T_c - T_c/2}{T_c}\right) \cdot \exp(j\phi_m) \cdot \exp[j2\pi f_c t] \quad (1)$$

where A is the amplitude of the pulse, f_c is the carrier frequency, and ϕ_m is the sequence of the phase code used.

2.1.2. SF waveform model

The SF radar transmits a burst of $N_p > 1$ pulses, whose carrier frequency monotonically increases from pulse to pulse by a fixed frequency step size denoted as Δf . For the $(i+1)^{\text{th}}$ pulse ($i \in \llbracket 0, N_p-1 \rrbracket$), the transmitted waveform is described as follows:

$$s_{tx,i}(t) = v_i(t) \cdot \exp[j2\pi f_i t] \quad (2)$$

with

$$v_i(t) = A \cdot \text{rect}\left(\frac{t - i \cdot T_r - T_p/2}{T_p}\right) \quad (3)$$

In (2), the carrier frequency of the $(i+1)^{\text{th}}$ transmitted pulse is given by:

$$f_i = f_c + \left(\frac{1 - N_p}{2} + i\right) \Delta f \quad (4)$$

where f_c is the central carrier frequency of the complete train of pulses. In addition, in (3), T_r denotes the pulse repetition interval.

2.1.3. SFPC waveform model

The SFPC waveform consists of a burst of N_p phase coded pulses whose carrier frequencies vary as in the case of the SF waveform. Therefore, it can be represented by (2) where $v_i(t)$ is given for $i \cdot T_r + m \cdot T_c \leq t < (i+1) \cdot T_r + m \cdot T_c$ and $i \in \llbracket 0, N_p-1 \rrbracket$ by:

$$v_i(t) = \sum_{m=0}^{M-1} A \cdot \text{rect}\left(\frac{t - m \cdot T_c - i \cdot T_r - T_c/2}{T_c}\right) \cdot \exp(j\phi_m) \quad (5)$$

In the FD algorithm, which is illustrated in the sequel, the discrete-time version of (5) is required where $T_s^{(Tx)}$ denotes the sampling time at the transmitter. Hence, (5) becomes:

$$v_i(n) = \sum_{m=0}^{M-1} A \cdot \text{rect}\left(\frac{n T_s^{(Tx)} - m \cdot T_c - i \cdot T_r - T_c/2}{T_c}\right) \cdot \exp(j\phi_m) \quad (6)$$

In (6), $n \in \llbracket 0, N-1 \rrbracket$ where $N = \frac{T_p}{T_s^{(Tx)}}$ denotes the number of samples associated with each transmitted pulse. In accordance with this arrangement, each sub-pulse is represented by N/M samples.

2.1.4. Received SF signal model

At the receiver, a demodulation process takes place to down-convert the signal to baseband. In the absence of noise³, the received SF signal for a stationary point target at range R can be written as follows:

$$\begin{aligned} s_{rx,i}(t) &= v_i\left(t - t_d\right) \cdot \exp\left[j2\pi f_i \cdot (t - t_d)\right] \\ &= v_i\left(t - \frac{2R}{c}\right) \cdot \exp\left[j2\pi f_i \cdot \left(t - \frac{2R}{c}\right)\right] \end{aligned} \quad (7)$$

where $t_d = \frac{2R}{c}$ and c is the speed of light. The reference signal used for the demodulation is defined by:

$$s_{ref,i}(t) = \exp[j2\pi f_i t] \quad (8)$$

The demodulated signal at the baseband is therefore given by:

$$\begin{aligned} s_{d,i}(t) &= s_{rx,i}(t) \cdot s_{ref,i}^*(t) \\ &= v_i\left(t - \frac{2R}{c}\right) \cdot \exp\left[-j2\pi f_i \cdot \frac{2R}{c}\right] \end{aligned} \quad (9)$$

As the baseband signal terms in (9) are associated with the range of the target, different algorithms can be exploited to produce the HRRP of the SF waveforms. Among them, the FD algorithm is presented in the following.

2.2. Processing chain based on the standard FD algorithm

The FD algorithm aims at reconstructing a large target reflectivity spectrum by coherently combining the individual spectra of the received narrow-band LFM pulses in the frequency domain [16]. In the following, the steps of the FD algorithm⁴ are briefly recalled:

1. $S_{d,i}(k)$, the DFT of the received samples associated with each pulse in (9) padded with $N-1$ zeros is computed, where $k \in \llbracket 0, 2N-2 \rrbracket$. The sampling frequency at the receiver satisfies in this case:

$$F_s^{(Rx)} = 2B_{inst} = \frac{F_s^{(Tx)}}{N_p} = \frac{B}{N_p} \quad (10)$$

In (10), $F_s^{(Tx)}$ denotes the sampling frequency at the transmitter and B denotes the total bandwidth of the waveform.

³For the sake of simplicity the noise is omitted, although in practical cases it exists. Its effect will be treated later on in the paper.

⁴The latter was based on the general waveform defined in (2), with $v_i(n) = A \cdot \text{rect}\left(\frac{n T_s^{(Tx)} - i \cdot T_r - T_p/2}{T_p}\right) \cdot \exp\left[j\pi \gamma (n T_s^{(Tx)})^2\right]$.

- An MF is applied to each pulse in the frequency domain. It consists in multiplying $S_{d,i}(k)$ by the conjugate of $V_i^{pad}(k)$, which is the DFT of $v_i(n)$ padded with $N - 1$ zeros, and it yields $Y_{r,i}(k)$.
- A compression filter is used to modify each resulting sub-spectrum $Y_{r,i}(k)$ by multiplying it by $H_i(k) = \frac{1}{|V_i^{pad}(k)|^2}$. This leads to:

$$Z_{r,i}(k) = \exp\left[-j2\pi\left(f_i + \frac{kF_s^{(R_x)}}{2N-1}\right)\frac{2R}{c}\right] \quad (11)$$

The magnitude of the synthesized spectrum obtained in (11) has a rectangular shape, *i.e.* $|Z_{r,i}(k)| = 1$.

- The sub-spectra in (11) are contiguously arranged to synthesize the whole spectrum.

$$\underline{Z}_{r,i} = [Z_{r,i}(0) Z_{r,i}(1) \dots Z_{r,i}(2N-2)] \quad (12)$$

The total concatenated spectrum can be represented as a row vector of size $(2N-1).N_p$ as follows:

$$\underline{Z}_{r,total} = [\underline{Z}_{r,0} \underline{Z}_{r,1} \dots \underline{Z}_{r,N_p-1}] \quad (13)$$

- $\underline{Z}_{r,total}$ is of interest to deduce the HRRP. As recalled in Appendix A, providing that $F_s^{(R_x)} = \Delta f$, the IDFT of the elements of the vector $\underline{Z}_{r,total}$ leads to:

$$|z_r(n)| = \frac{1}{(2N-1).N_p} \left| \frac{\sin\left[N_p\pi\left(F_s^{(R_x)}\frac{2R}{c} - \frac{n}{N_p}\right)\right]}{\sin\left[\frac{\pi}{2N-1}\left(F_s^{(R_x)}\frac{2R}{c} - \frac{n}{N_p}\right)\right]} \right| \quad (14)$$

where $n \in \llbracket 0, (2N-1).N_p - 1 \rrbracket$ and $|z_r(n)|$ has its maximum equal to 1 when $n = \frac{2RF_s^{(R_x)}N_p}{c} = t_d F_s^{(R_x)} N_p$.

Due to (14), amplitude weighting can be applied to reduce the range sidelobes. It consists in multiplying (13) by another row vector \underline{W} of the same length containing the spectrum of a shaping window, such as Hanning.

$$\underline{G}_{r,total} = \underline{Z}_{r,total} \cdot * \underline{W} \quad (15)$$

An IDFT is finally applied to the synthesized spectrum in (15) to create the HRRP.

2.3. Performance measures

Four performance measures are considered.

- The **peak sidelobe ratio** (PSLR) is given by:

$$PSLR = 20\log\left[\frac{\max(\text{sidelobe peak})}{\text{mainlobe peak}}\right] \quad (16)$$

The best performance in terms of PSLR mitigates the masking effect of nearby targets and increases the useful dynamic range.

- The **integrated sidelobe ratio** (ISLR) is given by:

$$ISLR = 10\log\left[\frac{\text{total energy in sidelobes}}{\text{energy in mainlobe}}\right] \quad (17)$$

The sidelobes which are less than T_p far away from the center of the mainlobe, on both sides of the mainlobe, are taken into consideration.

- The **minimum range** (R_{min}) represents the minimum range through which the targets can be detected by the radar. It is directly proportional to the pulse width:

$$R_{min} = \frac{cT_p}{2} \quad (18)$$

- The **range resolution** (R_{res}) is the separation between the peak and the first null of the range profile. R_{res} is inversely proportional to B_{eff} .

$$R_{res} = \frac{c}{2B_{eff}} \quad (19)$$

It reflects the capability of the radar to separate two closely spaced targets. Table. 1 summarizes the relationship between B_{inst} , B and B_{eff} for various waveforms.

Table 1: Relation between the bandwidths of different waveforms

Waveform	B_{inst}	B	B_{eff}
SCPC	M/T_p	$2M/T_p$	$B/2$
SF	$1/T_p$	$(N_p-1)\Delta F + 2B_{inst}$	$B/2$
SFPC	M/T_p	$(N_p-1)\Delta F + 2B_{inst}$	$B/2$

The level of significance given for each performance measure, especially the PSLR and the ISLR, depends on the surrounding environment. Whenever the received signal is disturbed by a distributed clutter environment, the ISLR is of high importance and should be maintained as low as possible to enable the detection of weak targets. For instance, it contributes to the multiplicative noise in SAR image [17]. However, if the received signal is disturbed by a strong discrete clutter, the PSLR is more critical to be kept low. Otherwise, sidelobes may be interpreted falsely as real targets [18].

In the following the modified SFPC waveform is presented.

3. The modified SFPC waveform

Let us first elaborate the background upon which the proposed waveform has been built. The way by which we construct the modified SFPC (M.SFPC) waveform has a great similarity and analogy with that of the SF-LFM waveform. To the best of our knowledge, researchers like Hamada [11] modulate the transmitted pulses of the SFPC

waveform with the same phase code. However, this arrangement is not useful whenever the FD algorithm is exploited since it leads to bad PSLR and ISLR. Accordingly, to solve this problem, we propose the M.SFPC waveform that follows the same methodology of the aforementioned SF-LFM waveform, and consequently improves both the PSLR and the ISLR.

This section deals with the steps done both at the transmitter and the receiver. They are presented for a non-overlapping scenario where $B_{inst} = \frac{B}{2N_p}$. A block diagram that illustrates the whole processing chain of the M.SFPC waveform is given in Fig. 1.

3.1. Generation of the modified SFPC waveform at the transmitter

3.1.1. Description of the different steps to be done

Without loss of generality, let us consider any single pulse from (6). For instance, for $i = 0$, it is given for $n \in \llbracket 0, N - 1 \rrbracket$ by:

$$v(n) = \sum_{m=0}^{M-1} A \cdot \text{rect}\left(\frac{nT_s^{(Tx)} - mT_c - T_c/2}{T_c}\right) \cdot \exp(j\phi_m) \quad (20)$$

where:

$$\frac{1}{T_s^{(Tx)}} = F_s^{(Tx)} = B \quad (21)$$

At this level, the following steps are carried out:

1. Apply a DFT to (20) to get $V(k)$.
2. Split $V(k)$ into N_p equal portions denoted as $P_l(k)$, where l is an integer that satisfies $l \in \llbracket 0, N_p - 1 \rrbracket$ and $k \in \llbracket 0, N - 1 \rrbracket$. If $N_p = 1$, this would correspond to a single phase coded pulse similar to the one given in (20). In the following, $N_p > 1$ and N is necessarily an integer multiple of N_p .

$$P_l(k) = \begin{cases} V(k) & \frac{lN}{N_p} \leq k \leq (l+1)\frac{N}{N_p} - 1 \\ 0 & \text{elsewhere} \end{cases} \quad (22)$$

The frequency band occupied by $P_l(k)$ is $\frac{F_s^{(Tx)}}{N_p}$.

3. Apply an IDFT to each separated portion $P_l(k)$. This leads to N_p sequences, $p_0(n), \dots, p_{N_p-1}(n)$, each of size N .
4. Scale the amplitudes of $\{p_l(n)\}_{l=0,1,\dots,N_p-1}$ as follows:

$$p_{s,l}(n) = \frac{1}{\sqrt{\frac{1}{N} \sum_{n=0}^{N-1} |p_l(n)|^2}} p_l(n) = \frac{1}{\alpha_l} p_l(n) \quad (23)$$

The train of pulses $\{p_{s,l}(n)\}_{l=0,\dots,N_p-1}$ represents the M.SFPC waveform. This step is necessary to guarantee that the powers of all transmitted pulses are equal.

5. Convert the discrete sequences $\{p_{s,l}(n)\}_{l=0,1,\dots,N_p-1}$ to the continuous-time domain by using a digital-to-analog converter (DAC).

6. Multiply the latter continuous-time domain pulses by $\exp[j2\pi f_c t]$ to frequency translate each portion by f_c . The resulting continuous-time signal transmitted through the antenna is hence given by:

$$s_{tx,l}(t) = \frac{1}{\alpha_l} p_l(t) \exp[j2\pi f_c t] \quad (24)$$

Furthermore, one has to prepare a version of the non-zero components of the spectra $P_0(k), \dots, P_{N_p-1}(k)$ centered at the zero frequency. These versions are not intended to be transmitted at all. They are saved in the memory of the radar to be used later on in the receiver part⁵. Thus, for $l \in \llbracket 0, N_p - 1 \rrbracket$, the reference signals are given by:

$$\begin{aligned} p_{ref,l}(n) &= p_l(n) \exp\left(-j2\pi \frac{(2l+1)B}{2N_p} \frac{n}{F_s^{(Tx)}}\right) \\ &\stackrel{(29)}{=} p_l(n) \exp\left(-j\pi \frac{2l+1}{N_p} n\right) \end{aligned} \quad (25)$$

Then, the resulting sequence associated with each portion is down-sampled by a factor N_p so that it is composed of $\frac{N}{N_p}$ samples. For $n \in \llbracket 0, \frac{N}{N_p} - 1 \rrbracket$, it is given by:

$$p_{ref,l}^{down}(n) = p_{ref,l}(n \cdot N_p) = p_l(n \cdot N_p) \exp\left(-j\pi(2l+1)n\right) \quad (26)$$

Finally, the output of the down-sampler is padded by $\frac{N}{N_p} - 1$ zeros to get the sequence $p_{ref,l}^{dopad}(n)$. Then, a DFT is applied to the latter sequence to obtain $P_{ref,l}^{dopad}(k)$, as shown in Fig. 1.

3.1.2. About the relation between $\mathbf{P}_{ref,l}^{dopad}(\mathbf{k})$ and $\mathbf{V}(\mathbf{k})$

Let us now find a relation between $P_{ref,l}^{dopad}(k)$ and $V(k)$. Given an N -length signal $x(n)$, it is known that the DFT of $\exp\left(-j2\pi \frac{mn}{N}\right) \cdot x(n)$ is equal to $X(k+m)$. Therefore, by combining (21) and (25), $P_{ref,l}(k)$ can be written as follows:

$$P_{ref,l}(k) = P_l\left(k + \frac{2l+1}{2} \frac{N}{N_p}\right) \quad (27)$$

Given Appendix C, one has:

$$\begin{aligned} P_{ref,l}^{dopad}(k) &= \sum_{k_1=0}^{\frac{N}{N_p}-1} P_{ref,l}^{down}(k_1) \\ &\cdot \exp\left(-j\pi \left(\frac{k}{2N - N_p} - \frac{k_1}{N}\right) (N - N_p)\right) \\ &\cdot \text{sinc}_{\frac{N}{N_p}}\left(2\pi N_p \left(\frac{k}{2N - N_p} - \frac{k_1}{N}\right)\right) \end{aligned} \quad (28)$$

⁵Normally, the received echoes are processed at the baseband to save the computational cost.

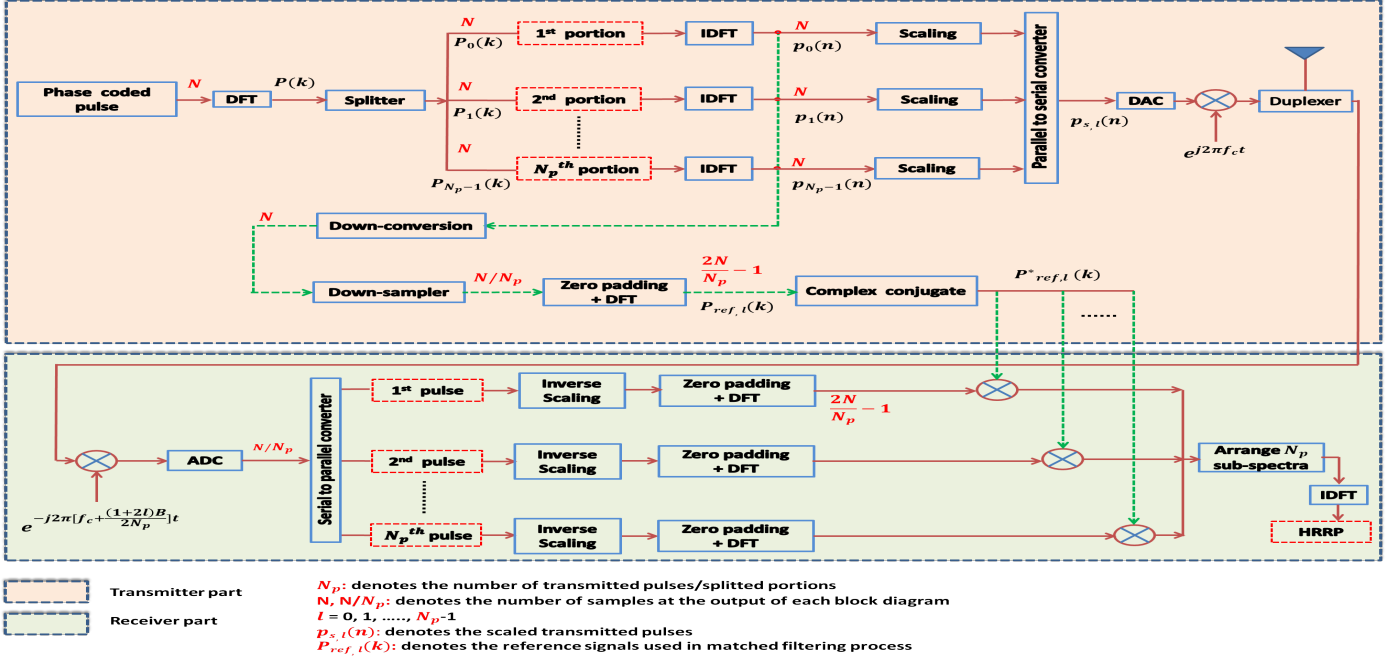


Figure 1: A block diagram showing the whole processing chain of the M.SFPC waveform at both transmitter and receiver sides

where the $psinc$ function is defined as follows:

$$psinc_{\frac{N}{N_p}}(\theta) = \frac{N_p}{N} \frac{\sin(\frac{N}{2}\theta)}{\sin(\frac{\theta}{2})} \quad (29)$$

Combining (22), (B.3), (27) and (28) leads to:

$$\begin{aligned}
 P_{ref,l}^{dopad}(k) &= \frac{1}{N_p} \sum_{k_1=0}^{\frac{2N}{N_p}-1} V\left(k_1 + \frac{2l+1}{2} \frac{N}{N_p}\right) \\
 &\cdot \exp\left(-j\pi\left(\frac{k}{2N-N_p} - \frac{k_1}{N}\right)(N-N_p)\right) \\
 &\cdot psinc_{\frac{N}{N_p}}\left(2\pi N_p\left(\frac{k}{2N-N_p} - \frac{k_1}{N}\right)\right) \\
 &+ \frac{1}{N_p} \sum_{k_1=\frac{2N}{N_p}}^{\frac{2N}{N_p}-1} V\left(k_1 + \frac{2N_p+2l-1}{2} \frac{N}{N_p}\right) \\
 &\cdot \exp\left(-j\pi\left(\frac{k}{2N-N_p} - \frac{k_1}{N}\right)(N-N_p)\right) \\
 &\cdot psinc_{\frac{N}{N_p}}\left(2\pi N_p\left(\frac{k}{2N-N_p} - \frac{k_1}{N}\right)\right)
 \end{aligned} \quad (30)$$

where $k \in \llbracket 0, \frac{2N}{N_p} - 2 \rrbracket$ and $k_1 \in \llbracket 0, \frac{N}{N_p} - 1 \rrbracket$.

These types of expressions are useful for the simulation of the receiving steps. It also shows the influences of the downsampling and the padding through the $psinc$ function.

3.2. Processing of the modified SFPC waveform at the receiver

3.2.1. Description of the different steps to be done

Due to the round trip path, the received signal corresponds to a version of the transmitted signal delayed by

the time t_d . In addition, the received signal is usually disturbed by additive disturbances containing the measurement white noise and the clutter. In the following and as done in subsection 2.2, they are not taken into account in order to focus the reader attention on the signal part. However, for completeness, the issues related to the noise will be addressed at the end of subsection 3.2.

Using (24), the "ideal" received signal is given by:

$$s_{rx,l}(t) = s_{tx,l}(t - t_d) = \frac{1}{\alpha_l} p_l(t - t_d) \exp(j2\pi f_c(t - t_d)) \quad (31)$$

The first step is to down-convert the received signal to the baseband. It is done by multiplying the l^{th} received pulse with $\exp(-j2\pi(f_c + \frac{(1+2l)B}{2N_p})t)$. The resulting signal is:

$$\begin{aligned}
 s_{bb,l}(t) &= \frac{1}{\alpha_l} p_l(t - t_d) \exp\left(-j2\pi\left(\frac{(1+2l)B}{2N_p}\right)t\right) \\
 &\times \exp(-j2\pi f_c t_d)
 \end{aligned} \quad (32)$$

Then, it is sampled at the sampling frequency $F_s^{(Rx)}$ defined in (10).

In this case, the number of samples that represent each received pulse is equal to $\frac{N}{N_p}$. For the sake of simplicity, let us address the toy example where the delay is strictly a multiple of the sampling period at the receiver ⁶, one has:

$$t_d = \frac{d}{F_s^{(Rx)}} = d \cdot T_s^{(Rx)} \quad (33)$$

⁶Otherwise some approximations would appear in the algorithm.

At this level, taking into account (10), (32), and (33), the l^{th} baseband received signal can be represented for $n \in \llbracket 0, \frac{N}{N_p} - 1 \rrbracket$ by:

$$s_{bb,l}(n) = \frac{1}{\alpha_l} p_l((n-d)N_p) \exp(-j\pi(1+2l)n) \exp(-j2\pi f_c \cdot d \cdot T_s^{(Rx)}) \quad (34)$$

Given (26), this leads to:

$$s_{bb,l}(n) = \frac{1}{\alpha_l} \cdot p_{ref,l}^{down}(n-d) \exp(-j\pi(1+2l)d) \exp(-j2\pi f_c \cdot d \cdot T_s^{(Rx)}) \quad (35)$$

Then, the following steps are carried out:

1. Apply an inverse scale to the result given in (35) by multiplying each received pulse by α_l . Hence, for $n \in \llbracket 0, \frac{N}{N_p} - 1 \rrbracket$, (35) becomes:

$$p_{ref,l}^{down}(n-d) \exp(-j2\pi f_c \cdot d \cdot T_s^{(Rx)}) \exp(-j\pi(1+2l)d) \quad (36)$$

2. Pad each sequence obtained in (36) by $\frac{N}{N_p} - 1$ zeros. This yields a vector of length $Q = \frac{2N}{N_p} - 1$ on which a Q -size DFT is applied. The result is given by:

$$P_{ref,l}^{dopad}(k) \exp(-j2\pi \frac{k}{Q} d) \exp(-j2\pi f_c \cdot d \cdot T_s^{(Rx)}) \cdot \exp(-j\pi(1+2l)d) \quad (37)$$

where $k \in \llbracket 0, \frac{2N}{N_p} - 2 \rrbracket$.

3. Apply an MF by multiplying each component of (37) by the complex conjugate of $P_{ref,l}^{dopad}(k)$. The output is given by:

$$Z_l(k) = |P_{ref,l}^{dopad}(k)|^2 \exp(-j2\pi \frac{k}{Q} d) \exp(-j2\pi f_c \cdot d \cdot T_s^{(Rx)}) \exp(-j\pi(1+2l)d) \quad (38)$$

where from (30) one has:

$$\begin{aligned} |P_{ref,l}^{dopad}(k)|^2 &= \frac{1}{N_p^2} \sum_{k_1=0}^{\frac{N}{2N_p}-1} \left| V\left(k_1 + \frac{2l+1}{2} \frac{N}{N_p}\right) \right|^2 \\ &\quad \cdot \text{sinc}^2_{\frac{N}{N_p}} \left(2\pi N_p \left(\frac{k}{2N-N_p} - \frac{k_1}{N} \right) \right) \\ &\quad + \frac{1}{N_p^2} \sum_{k_1=\frac{N}{2N_p}}^{\frac{N}{N_p}-1} \left| V\left(k_1 + \frac{2N_p+2l-1}{2} \frac{N}{N_p}\right) \right|^2 \\ &\quad \cdot \text{sinc}^2_{\frac{N}{N_p}} \left(2\pi N_p \left(\frac{k}{2N-N_p} - \frac{k_1}{N} \right) \right) \end{aligned} \quad (39)$$

The values in (38) are then stored in a vector of length $Q = \frac{2N}{N_p} - 1$:

$$\underline{Z}_l = [Z_l(0) Z_l(1) \dots Z_l(Q-1)] \quad (40)$$

4. Construct the whole spectrum by arranging the N_p sub-spectra contiguously. The total concatenated spectrum is represented by a row vector of size $N_p Q = 2N - N_p$ as follows:

$$\underline{Z}_{total} = [Z_0 Z_1 \dots Z_{N_p-1}] \quad (41)$$

Alternatively, this frequency shift can be achieved by multiplying the time domain version of (38) with a linear phase ramp. However, using a cut and paste method in the frequency domain, as it is done here, results in a much more efficient algorithm [1].

5. To produce the HRRP, apply an IDFT to (41) yields:

$$z(n) = \frac{1}{N_p Q} \sum_{l=0}^{N_p-1} \sum_{k=0}^{Q-1} Z_{total}(lQ+k) \exp\left(j \frac{2\pi(lQ+k)n}{N_p Q}\right) \quad (42)$$

where $Z_{total}(lQ+k)$ is the $(lQ+k)^{th}$ element of \underline{Z}_{total} . A zero padding may be done in the frequency domain to force power of 2-size IFFT, or to interpolate further the HRRP to get a better view. It should be noted that plotting the HRRP by directly using (39) and (42) constitutes a milestone to validate the results of the simulation section.

3.2.2. Remark about the impact of the compression filter in the presence of noise

Let us now assume that a white Gaussian noise is added to the received signals. Hence, (40) becomes:

$$s_{rx,l}(t) = s_{tx,l}(t-t_d) + u_l(t) \quad (43)$$

$$= \frac{1}{\alpha_l} p_l(t-t_d) \exp(j2\pi f_c(t-t_d)) + u_l(t) \quad (44)$$

where $u_l(t)$ represents the Gaussian noise in the l^{th} pulse. Following the same mathematical developments done after (40), the expressions given in (37) and (38) become respectively:

$$\begin{aligned} &P_{ref,l}^{dopad}(k) \exp(-j2\pi \frac{k}{Q} d) \exp(-j2\pi f_c \cdot d \cdot T_s^{(Rx)}) \\ &\cdot \exp(-j\pi(1+2l)d) + \tilde{U}_l(k) \end{aligned} \quad (45)$$

where $\tilde{U}_l(k)$ is the DFT of the baseband noise at the output of the processing chain,

and

$$Z_l(k) = |P_{ref,l}^{dopad}(k)|^2 \exp(-j2\pi \frac{k}{Q} d) \exp(-j2\pi f_c \cdot d \cdot T_s^{(Rx)}) \exp(-j\pi(1+2l)d) + \tilde{U}_l(k) \cdot P_{ref,l}^{dopad}(k)^* \quad (46)$$

At this stage, let us apply the compression filtering by dividing each sub-spectrum $Z_l(k)$ by $|P_{ref,l}^{dopad}(k)|^2$. Hence,

(46) becomes:

$$Z_l(k) = \exp\left(-j2\pi\frac{k}{Q}d\right)\exp\left(-j2\pi f_c.d.T_s^{(Rx)}\right) \quad (47)$$

$$\cdot \exp\left(-j\pi(1+2l)d\right) + \frac{\tilde{U}_l(k)}{P_{ref,l}^{dopad}(k)}$$

Phase coded pulses may exhibit small values in their spectrum at certain frequencies (see, for instance, Fig. 3). At the bins that represent these frequencies, $\frac{\tilde{U}_l(k)}{P_{ref,l}^{dopad}(k)}$ have large values. As a consequence, high peaks appear in the reconstructed spectrum. As they produce artifacts in the HRRP, the PSLR and ISLR deteriorate. Therefore, processing the SFPC waveform with the FD algorithm leads to undesirable performance in terms of PLSR and ISLR. As an alternative, a modified FD algorithm can be used where the compression filter is avoided.

3.3. Removing the constraints to choose $F_s^{(Tx)}$ and N_p

Splitting the original spectrum into N_p equal portions cannot be done when $F_s^{(Tx)}/N_p$ is not an integer. To address this problem, there are two possibilities:

1. **Decomposing the spectrum into N_p portions of unequal size:** In this case, each portion has a different bandwidth. Following this methodology, the spectrum can be split into any number of portions without worrying about the ratio $F_s^{(Tx)}/N_p$. However, at the receiver, the pulses would have different bandwidths. The sampling frequency would be either confined to the largest bandwidth of the portions or modified for each received echo.
2. **Resorting to an overlapping methodology:** The spectrum is still split into N_p equal portions, but the bandwidth of each portion is augmented and overlaps with its neighbor. The percentage of the overlap is the same between every two successive portions. By doing so, N_p is maintained within the CPI whereas $F_s^{(Rx)}$ increases. The larger the overlapping, the higher the $F_s^{(Rx)}$. Following this methodology, as the second equality in (10) no longer holds, some simplifications done for the equations at the receiver part are no longer valid. In this case, (36), (37), and (38) become respectively:

$$\pm p_{ref,l}^{down}(n-d)\exp\left(-j2\pi f_c.d.T_s^{(Rx)}\right) \quad (48)$$

$$\cdot \exp\left(-j\pi\frac{(1+2l)B.d.T_s^{(Rx)}}{N_p}\right)$$

$$\pm P_{ref,l}^{dopad}(k)\exp\left(-j2\pi\frac{k}{Q}d\right)\exp\left(-j2\pi f_c.d.T_s^{(Rx)}\right) \quad (49)$$

$$\cdot \exp\left(-j\pi\frac{(1+2l)B.d.T_s^{(Rx)}}{N_p}\right)$$

$$\pm |P_{ref,l}^{dopad}(k)|^2 \exp\left(-j2\pi\frac{k}{Q}d\right)\exp\left(-j2\pi f_c.d.T_s^{(Rx)}\right) \quad (50)$$

$$\cdot \exp\left(-j\pi\frac{(1+2l)B.d.T_s^{(Rx)}}{N_p}\right)$$

As a consequence, a trade-off has to be found in the selection of the methodology that would be followed for splitting the original spectrum. Selection relies on the specified application and the limitation one would have in terms of $F_s^{(Rx)}$.

3.4. Comments

1. **About the envelope of the M.SFPC:** In the traditional radar waveforms, the transmitted pulses have a constant envelope even though they may have a phase or frequency modulation in the context of an intra-pulse modulation. However, in our M.SFPC waveform, the resulting samples of each transmitted pulse have not only arbitrary phases but also arbitrary amplitudes, as shown in Fig. 2. Having a non-constant envelope is a common feature of some proposed waveforms, e.g. the orthogonal frequency division multiplexing (OFDM), and the hybrid NLFM. [19] [20] [21].

2. **About a trade-off between R_{min} and B_{inst} :** Radar engineers are always interested in using the minimal possible pulse width. In order to obtain high PSLRs with phase coded pulses, it is better to use polyphase codes of large length M . They lead to a trade-off between R_{min} and B_{inst} . On the one hand, exploiting these long codes with a fixed pulse width leads to a dramatic augmentation of B_{inst} because the latter is proportional to M (see Table 1). On the other hand, if we augment the pulse width to grasp this long code, R_{min} increases according to (18). As a consequence, a trade-off has also to be found between the minimum range and the instantaneous bandwidth. This is the case of the SFPC waveform.

With the M.SFPC waveform and thanks to the methodology followed at the transmitting and receiving sides, the polyphase codes with large length M can be exploited while each pulse of the M.SFPC waveform still has the same width as the original pulse from which it is derived. Hence, for a certain value of B_{inst} , the minimum range of the waveform is smaller than that of the SFPC waveform.

3. **About the computational cost of M.SFPC vs. SFPC:** For a fair comparison, N_p and B_{inst} are set at the same values for both M.SFPC and SFPC. As a consequence, each pulse of the SFPC waveforms consists of N samples whereas each pulse of the M.SFPC waveform consists of $\frac{N}{N_p}$ samples. Table. 2 summarizes the computational cost of each step for both

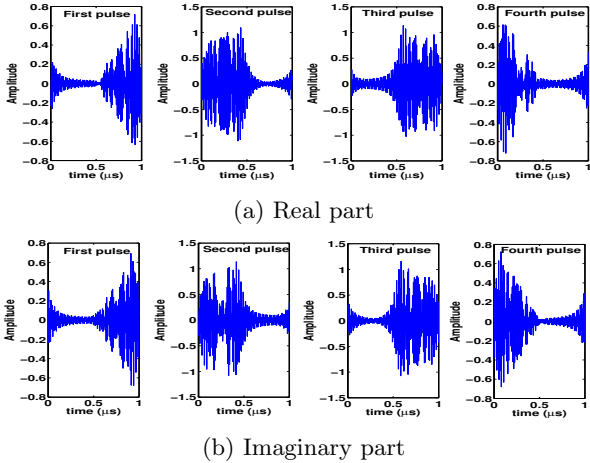


Figure 2: Real and imaginary parts of the M.SFPC waveform where the spectrum is split into four portions

Table 2: The computational cost of the M.SFPC and SFPC waveforms at the transmitter and receiver sides. / is used when no computational cost is required

Steps	Transmitter		Receiver	
	SFPC	M.SFPC	SFPC	M.SFPC
1	/	$O(N^2)$	$O(N_p \cdot N^2)$	$O(N)$
2	/	/	$O(N_p(2N - 1))$	$O(\frac{(2N - N_p)^2}{N_p})$
3	/	$O((N \cdot N_p)^2)$	$O(N_p(2N - 1))$	$O(2N - N_p)$
4	/	$O(NN_p)$	/	/
5	/	/	$O(N_p(2N - 1))$	$O((2N - N_p)^2)$
6	/	/	$O(N_p^2(2N - 1)^2)$	/

the M.SFPC and the SFPC at the transmitter and receiver sides.

On the one hand, at the transmitter side, generating the transmitted signal for the SFPC waveform is straightforward and avoids all the procedure done for the M.SFPC waveform. However, all the steps at the transmitter should be executed only once. When the waveform is generated for the first time, the resulting samples are saved in the memory of the radar to be utilized later on for other transmissions. As a consequence, the computational burden at the transmitter is almost negligible compared with that of the receiver. Normally, radar engineers are interested in the latter rather than the former. This is due to the fact that all the steps at the receiver should be repeated every time an echo arrives at its front end. On the other hand, at the receiver side, given Table. 2, the addition of the computational power of the whole steps of each waveform reveals that the M.SFPC waveform requires less computational power than the SFPC waveform. Finally, in our M.SFPC waveform, the generated pulses are multiplied by the same carrier signal which eases the operation of the oscillator whereas in the SFPC waveform the frequency of the carrier signal varies in a fixed step from pulse to pulse.

4. **About the relation between N_p and CPI:** It is important that all the N_p pulses that carry the different portions of the split spectrum are transmitted within the CPI. This highly depends on the velocity of the target. If the target is fixed or moving slowly, the number N_p of split portions of the spectrum can be large, and consequently, a better performance is achieved. However, if the target is moving fast, then N_p should be relatively small in order to guarantee that all the transmitted pulses lie within the CPI. Otherwise, the radar will not be able to receive all the echoes within the CPI. One of the possible solutions for this issue is to resort to compressed sensing techniques that have been proposed to deal with such scenarios where sparsity in the collected data exists [22] [23].

4. Simulations and results

In this section, some features such as the magnitude spectrum and the range resolution of the M.SFPC waveform are investigated first. Then, comparisons of the M.SFPC waveform with SCPC and SFPC waveforms are presented.

4.1. The magnitude spectrum of M.SFPC waveform

At the receiver, as mentioned in subsection 3.2, each pulse is padded by zeros followed by an MF in the frequency domain. Let us analyze the influence of the zero-padding process on the reconstructed spectrum. For this purpose, suppose that there is a single pulse phase coded with P4 of length $M = 100$. Fig. 3 represents its magnitude spectrum obtained by two approaches: one by the DFT without padding and the other by the DFT with padding. It reveals that the discrete spectra are quasi-symmetric. Let us now apply our methodology, illustrated in subsection 3.1, by splitting the discrete magnitude spectrum presented in red in Fig. 3 into $N_p = 4, 10, 20, 50$ portions. In Fig. 4, for each value of N_p , the reconstructed spectrum is presented. It is obvious that after reconstructing the spectrum, the quasi-symmetric feature is lost. When N_p increases, the reconstructed spectrum differs more and more from the original one. This is due to the fact that applying the MF to the single received echo of the SCPC that is zero padded yields a different result from zero padding the corresponding received-echoes of the M.SFPC while applying the split MF.

4.2. M.SFPC waveform vs. SCPC waveform

4.2.1. R_{res} of the M.SFPC waveform

Let us now investigate the capability of our M.SFPC waveform to obtain the range resolution of the SCPC waveform. Again, a polyphase P4 code with length $M = 100$ is used. In Fig. 5, we present the HRRP of a stationary point target located at range $R = 240$ m when $N_p = 4, 10, 20$, and 40. For $N_p = 10, 20$ and 40, $R_{res} = 1.5$ m which is equal to the range resolution of the SCPC waveform. When $N_p = 4$, R_{res} for the M.SFPC waveform is slightly larger than the range resolution of the SCPC waveform.

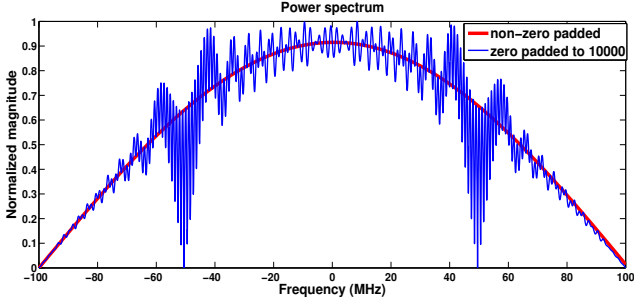
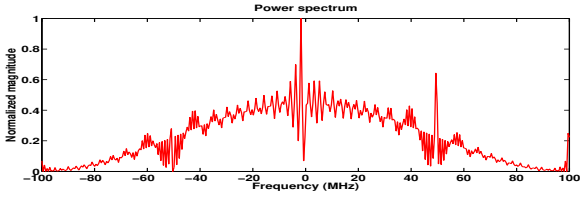
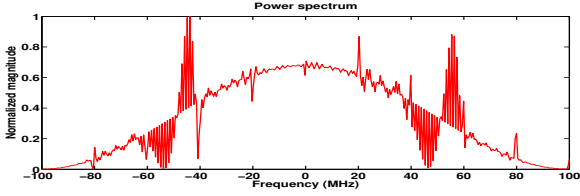


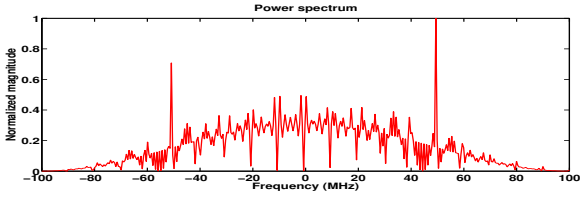
Figure 3: The power spectrum of polyphase P4 whose length is $M = 100$, with or without zero-padding



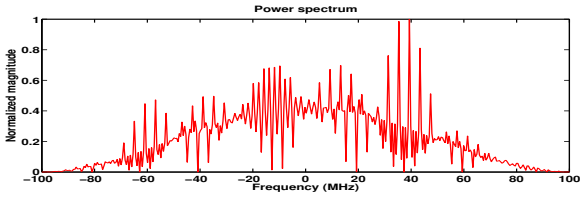
(a)



(b)



(c)



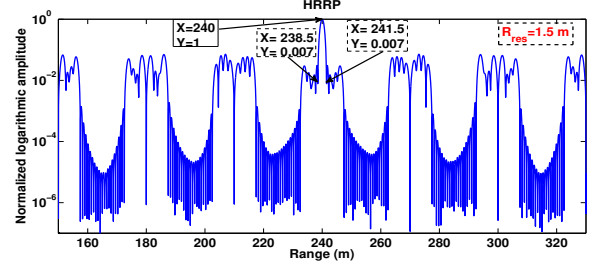
(d)

Figure 4: Reconstructed power spectrum which corresponds to the concatenation of $|P_{ref,l}^{dopad}(k)|^2$ (a) $N_p = 4$, (b) $N_p = 10$, (c) $N_p = 20$, and (d) $N_p = 50$.

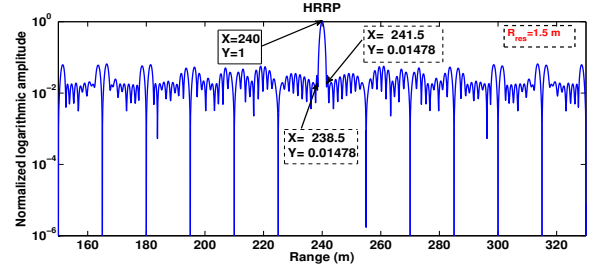
4.2.2. Introduction including simulation protocol

Our purpose is to study the performance of the M.SFPC waveform with stationary targets. An additive white Gaussian noise (AWGN) is considered at the receiver, leading to a specific SNR. Some of the common parameters used in the whole subsection are given in Table 3, while the others are introduced gradually. In all the simulations, two cases (non-overlap and overlap) are addressed.

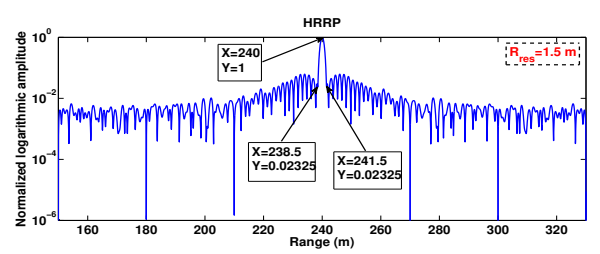
At the receiver, the SCPC waveform is processed by MF



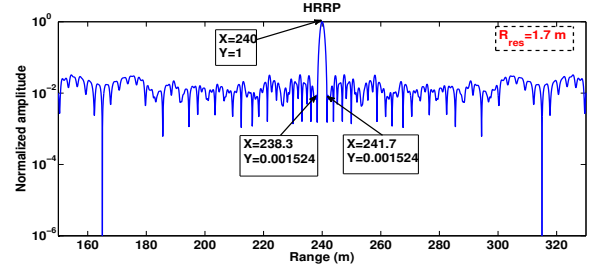
(a)



(b)



(c)



(d)

Figure 5: HRRP of the M.SFPC waveform when (a) $N_p = 40$, (b) $N_p = 20$, (c) $N_p = 10$, and (d) $N_p = 4$.

Table 3: General Parameters used in the simulation section

Parameter	Value
Pulse repetition frequency (PRF)	250 Hz
Carrier frequency (f_c)	3 GHz
Pulse width (T_p)	1 μ s

since it consists of a single carrier whereas the steps given in subsection 3.2 are done for the M.SFPC waveform. Therefore, as $F_s^{(Rx)}$ is proportional to the bandwidth of the received signal, the sampling frequency at the receiver for the M.SFPC waveform is N_p times smaller than that of

the SCPC. Even if this comparison could be unfair due to this difference, we propose to analyze how much the PSLR and the ISLR vary. In the first illustration, the spectrum is split into non-overlapping portions, whereas in the second one, it is split into overlapping portions.

Simulation protocol: The SNR varies from -5 dB to 30 dB with a step equal to 1 dB. For each SNR, 7000 independent realizations of the noise are generated. The SNR is defined as the ratio between the power of the SCPC pulse, denoted as \mathbf{P}^{SCPC} , and the variance of the noise, σ_n^2 .

$$SNR = 10\log_{10}\left(\frac{\mathbf{P}^{SCPC}}{\sigma_n^2}\right) \quad (51)$$

For the non-overlapping case and for a fair comparison, the sum of the powers of the N_p pulses of the M.SFPC waveform is equal to \mathbf{P}^{SCPC} . Hence, even when N_p changes, the sum of the power of all pulses is kept fixed. As for the phase codes used in this illustration, both P4 with length $M = 100$ ($B = 200$ MHz) and polyphase Barker with length $M = 54$ ($B = 108$ MHz) are considered.

For the overlapping case, the percentage of the overlap is set at 50%. The total number of samples of the M.SFPC waveform in this case is larger than that of the SCPC pulse by a factor of 1.5. Thus, for a fair comparison between both waveforms, the sum of the energy of N_p pulses of the M.SFPC waveform is equal to the energy of the SCPC pulse. Furthermore, only P4 with length $M = 100$ ($B = 200$ MHz) and $T_p = 1 \mu s$ are considered for all the simulations in this illustration. Hence, both R_{min} and R_{res} are fixed.

4.2.3. Results and comments

The M.SFPC waveform with non-overlapping portions versus SCPC

Let us now study the evolutions of the PSLR and the ISLR with respect to the SNR. According to Fig. 6, the mean value of the PSLR for both waveforms gets worse as the SNR decreases. At very low SNR, the mean of the PSLR of the M.SFPC waveform is 1.5 dB worse than that of the SCPC for $N_p \neq 2$. However, at high SNR the mean of the PSLR of the M.SFPC waveform is highly dependent on N_p . This difference appears since an MF is applied separately to each received pulse. Furthermore, the ability of the M.SFPC waveform with $N_p = 4$ to outperform the SCPC waveform comes at the expense of an increase of the range resolution, as shown in Fig. 5-a. The good performance is mainly due to the interaction between two phenomena: First, the MF is applied to each pulse separately instead of jointly applying it to all the received echoes. Second, the cyclic-autocorrelation of the P4 code has zero sidelobes. The last feature has been exploited recently to separate overlapping echoes in weather radar [24]. In Fig. 8, the evolution of the PSLR of the M.SFPC using polyphase Barker code is presented. The latter code does not exhibit the zero-sidelobes feature. It reveals that the M.SFPC waveform is no longer capable of outperforming

the SCPC waveform. This result confirms our aforementioned interpretation.

In the same context, Fig. 7 provides the mean value of the ISLR at different SNR for both waveforms using P4 code. At very low SNR, the value of the ISLR of the M.SFPC waveform is 2 dB worse than that of the SCPC waveform for $N_p \neq 2$. However, at high SNR, this amount varies with N_p .

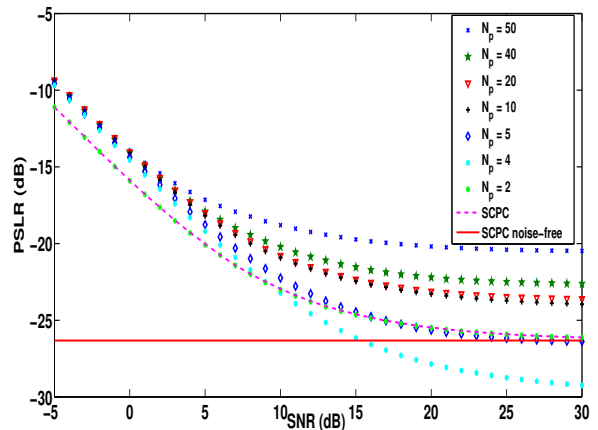


Figure 6: Mean value of PSLR versus SNR using N_p portions of polyphase P4 ($M = 100$)

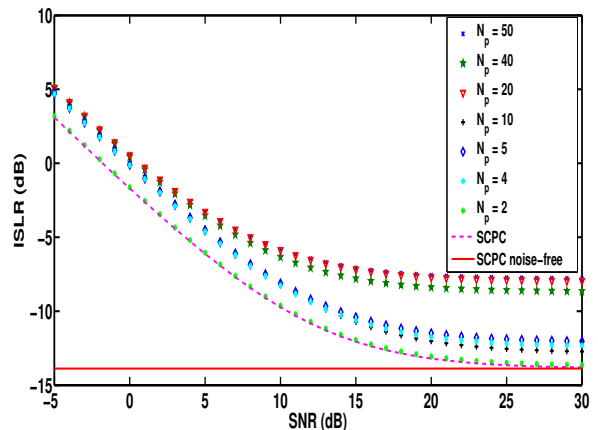


Figure 7: Mean value of ISLR versus SNR using N_p portions of polyphase P4 ($M = 100$)

The M.SFPC waveform with overlapping portions vs. SCPC waveform

Let us now investigate the performance of our M.SFPC waveform when an overlap between different portions exists. For this purpose, a set of Monte-Carlo simulations is carried out in which a P4 code is used as an intra-pulse modulation. In Fig. 9 and Fig. 10, the mean values of the PSLR and the ISLR of the M.SFPC waveform are respectively presented as functions of the SNR. The

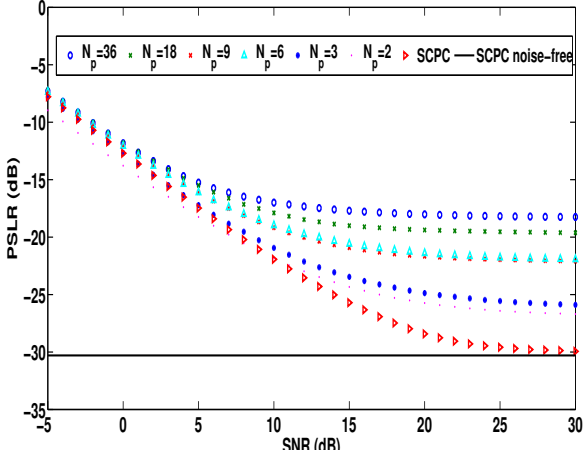


Figure 8: Mean value of the PSLR versus SNR using N_p portions of polyphase Barker ($M = 54$)

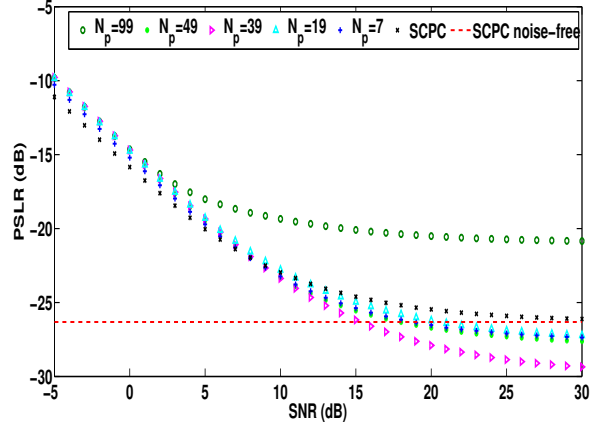


Figure 9: Mean value of the PSLR versus SNR using N_p overlapping portions of polyphase P4 ($M = 100$)

PSLR ranges between -29 dB for $N_p = 39$ and -21 dB for $N_p = 99$. Using the overlapping between the transmitted portions offers the possibility to enhance the performance compared to the non overlapping scenario. For instance, at SNR = 30 dB, when $N_p = 50$ for the non-overlapping scenario and $N_p = 49$ for the overlapping one, the gain in terms of PSLR is around 6.8 dB. Although the number of transmitted pulses is almost the same in both scenarios, B_{inst} for each transmitted portion in the non-overlapping scenario is equal to 4 MHz, whereas it is set at 8 MHz in the overlapping one. Therefore, this improvement comes at the expense of increasing the sampling frequency at the receiver. Moreover, as with non-overlapping portions, the PSLR of the M.SFPC waveform is larger than that of the SCPC waveform due to the same reasons. It is obvious that at low SNR, both the PSLR and ISLR of the M.SFPC waveform for the different number of portions N_p converge to the same value.

In order to shed light more on the powerfulness of the overlapping scenario in attaining PSLR and ISLR values better than those obtained with the non-overlapping one, we present a summary of different simulations we have conducted in Table. 4. In every row of this table, the value of N_p for the overlapping and the corresponding non-overlapping cases are carefully chosen. For $N_p = 9$ in the overlapping case which requires $F_s^{(Rx)} = 40$ MHz, we choose two corresponding values of N_p for the non-overlapping case: $N_p = 5$ which is almost twice smaller but used with the same sampling frequency at the receiver and $N_p = 10$ which requires almost the same number of portions but used with the sampling frequency which is twice smaller. Similar comments can be drawn for the other three cases presented in the table. Given the results presented in table 4, the overlapping scenario outperforms the non-overlapping one, in terms of PSLR and ISLR. The tax to be paid is either a higher $F_s^{(Rx)}$ or a larger N_p .

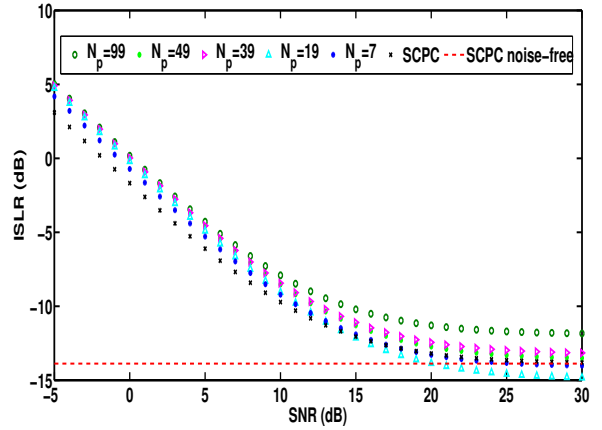


Figure 10: Mean value of the ISLR versus SNR using N_p overlapping portions of polyphase P4 ($M = 100$)

Table 4: PSLR and ISLR of the M.SFPC waveform for overlapping vs. corresponding non-overlapping cases, using polyphase P4 ($M=100$) in a noiseless scenario

N_p	$F_s^{(Rx)}$ (MHz)	PSLR (dB)	ISLR (dB)	50% Overlap
5	40	-26.46	-12.1	No
9	40	-27.04	-15.5	Yes
10	20	-24.15	-12.8	No
10	20	-24.15	-12.8	No
19	20	-27.52	-15.76	Yes
20	10	-23.7	-7.9	No
20	10	-23.7	-7.9	No
39	10	-29.63	-13.54	Yes
40	5	-22.62	-8.65	No
50	4	-20.5	-7.8	No
99	4	-20.96	-11.86	Yes
100	2	-12	-5.94	No

4.3. Our modified SFPC waveform vs. SFPC waveform

4.3.1. Introduction including simulation protocol

In this section, the performance of the M.SFPC waveform as defined in the previous subsection is compared with that of the SFPC waveform. Both the IFFT and the FD algorithms are used, because the first one is usually considered whereas the second has not yet been applied in the literature with the SFPC waveform.

Simulation protocol: The SNR in both illustrations is defined by:

$$SNR = 10\log_{10}\left(\frac{\mathbf{P}_l^{SFPC}}{\sigma_n^2}\right) = 10\log_{10}\left(\frac{\mathbf{P}_l^{M.SFPC}}{\sigma_n^2}\right) \quad (52)$$

where \mathbf{P}_l^{SFPC} and $\mathbf{P}_l^{M.SFPC}$ respectively denote the power of the l^{th} pulse of SFPC and M.SFPC waveforms. For a fair comparison in both illustrations, the following equality holds true:

$$\sum_{l=0}^{N_p-1} \mathbf{P}_l^{SFPC} = \sum_{l=0}^{N_p-1} \mathbf{P}_l^{M.SFPC} \quad \forall N_p \quad (53)$$

Furthermore, the power of each transmitted pulse in both waveforms is kept fixed even when N_p changes. This is different from what has been implemented in subsection 4.2.

Concerning the parameters and the phase codes used, there are some variations depending on the algorithm used at the receiver:

1. The case of the FD algorithm: Polyphase Barker code with length $M = 60$ is used instead of P4 as an intra-pulse modulation. The reason for this selection is due to the fact that in the FD algorithm, the output of the MF is multiplied by the inverse of the magnitude spectrum (See section 2.2, step 3). This arrangement cannot work properly with polyphase codes, such as P4, because they exhibit small values in their magnitude spectra, as illustrated previously in 3.2.2. The polyphase Barker code is one of the codes that does not exhibit small values in its spectrum. The parameters of each waveform are given in Table. 5. For a fair comparison, B_{inst} for both waveforms should be the same. Moreover, this table shows that B_{eff} is also the same. This has been achieved by making 50% overlapping between the spectra of the different pulses of the SFPC waveform at the transmitter. At the receiver, the spectrum of each received echo of the SFPC waveform is multiplied by a rectangular window of width $B/(2N_p)$. Hence, at the receiver, only half of the transmitted spectrum of each received echo of the SFPC waveform is exploited. This methodology is used for two reasons: To guarantee a fair comparison between both waveforms by maintaining the same B_{eff} , and to reduce the ISLR of the SFPC waveform as much as possible.

2. The case of the IFFT algorithm: The parameters used in this simulation are given in Table. 6. Again, the parameters are selected so that B_{inst} is the same for both waveforms. Moreover, the polyphase P4 code with length $M = 100$ is used.

4.3.2. Results and comments

Modified SFPC versus SFPC using FD algorithm

First, in Fig. 11, the HRRP of the SFPC waveform in the absence of noise when $N_p = 10$ is presented. Then, in Fig. 12a, the PSLR versus SNR for both waveforms are depicted for different numbers of transmitted pulses. The PSLR of the SFPC waveform cannot exceed -13.5 dB, in the best case with the absence of noise. This is because its spectrum is transformed into a rectangular form, after applying the compression filter. Therefore, its PSLR is significantly worse than that of the M.SFPC at the whole SNR range, no matter what N_p is. In Fig. 12b the ISLR of both waveforms is shown. It is obvious that the M.SFPC substantially outperforms the SFPC at low to moderate SNR, whereas the performance is equivalent at high SNR and large N_p . Furthermore, Table. 5 reveals that the pulse width in M.SFPC does not vary with N_p . It exhibits a smaller minimum range compared with the SFPC. This is because the pulse width of the latter waveform grows with N_p . The minimum range must be as small as possible for radars that search for targets at a close range. It turns out that the exploitation of the FD algorithm with the SFPC is not favorable due to the non-rectangular shape of any phase coded pulse. As a consequence, the M.SFPC waveform is considered as an alternative to the SFPC waveform when the FD algorithm is used.

Table 5: Parameters for contrasting M.SFPC and SFPC waveforms using the FD algorithm. Polyphase Barker ($M = 60$) is used as an intra-pulse modulation

Parameter	M.SFPC	SFPC		
	$\forall N_p$	$N_p = 10$	$N_p = 20$	$N_p = 30$
T_p (μs)	1	10	20	30
B_{inst} (MHz)	$\frac{B}{2N_p}$	6	3	2
$F_s^{(Rx)}$ (MHz)	$\frac{B}{N_p}$	12	6	4
Δf (MHz)	$\frac{B}{N_p}$	6	3	2
B (MHz)	120	120	120	120
B_{eff} (MHz)	60	60	60	60
R_{res} (m)	2.5	2.5	2.5	2.5
R_{min} (m)	150	1500	3000	4500

Modified SFPC vs. SFPC using IFFT algorithm

In Fig. 13a and Fig. 13b, the evolutions of the mean value of the PSLR and ISLR of both waveforms for various

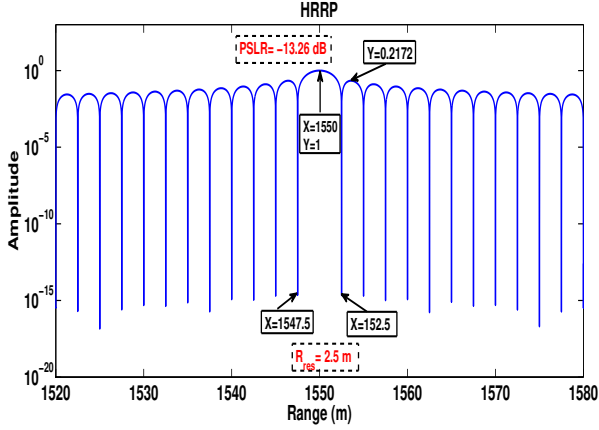
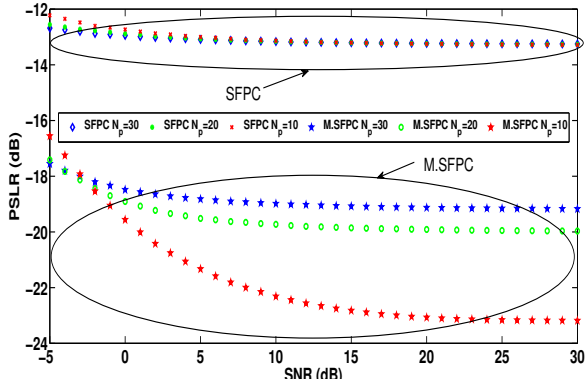
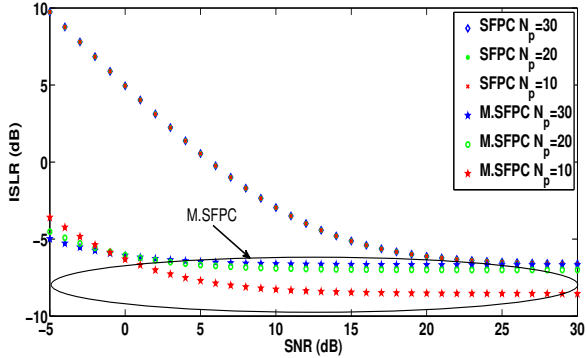


Figure 11: HRRP of SFPC waveform treated using the FD algorithm. The phase code used is polyphase Barker with $M = 60$.



(a) Mean value of PSLR



(b) Mean value of ISLR

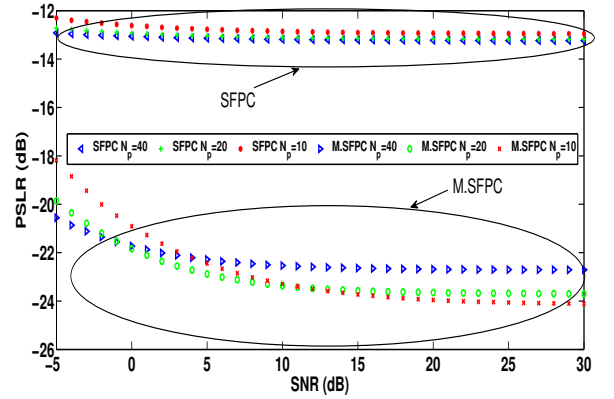
Figure 12: Mean values of the PSLR and ISLR versus SNR for the SFPC, treated with FD algorithm, and M.SFPC waveforms using polyphase Barker ($M = 60$).

N_p are presented respectively. Fig. 13a shows clearly the enhancement of the PSLR of the M.SFPC waveform compared to that of the SFPC waveform. As for the ISLR, the results are highly dependent on N_p . Hence, the M.SFPC waveform outperforms the SFPC for certain values of N_p , and the converse occurs for other values. Looking at both waveforms from another viewpoint, the range resolution for the SFPC waveform is twice better than that of the

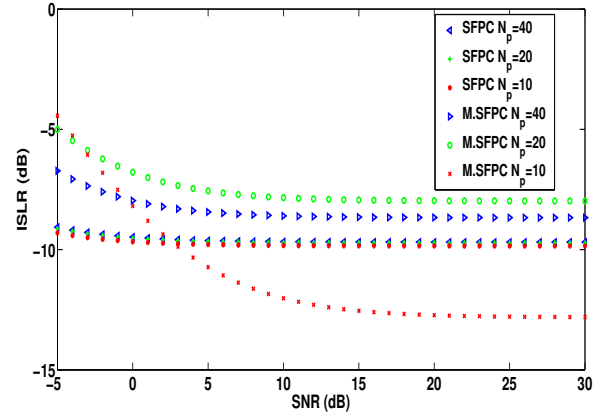
M.SFPC. However, the minimum range of the M.SFPC waveform is kept constant for any value of N_p whereas that of the SFPC waveform varies with the selected N_p . The larger N_p is, the longer R_{min} is. See Table. 6.

Table 6: Parameters for contrasting M.SFPC and SFPC waveforms using IFFT algorithm. Polyphase P4 is used as an intra-pulse modulation

Parameter	M.SFPC	SFPC		
	$\forall N_p$	$N_p = 10$	$N_p = 20$	$N_p = 40$
T_p (μs)	1	10	20	40
B_{inst} (MHz)	$\frac{B}{2N_p}$	10	5	2.5
$F_s^{(Rx)}$ (MHz)	$\frac{B}{N_p}$	20	10	5
Δf (MHz)	$\frac{B}{N_p}$	20	10	5
B (MHz)	200	200	200	200
B_{eff} (MHz)	100	200	200	200
R_{res} (m)	1.5	0.75	0.75	0.75
R_{min} (m)	150	1500	3000	6000



(a) Mean value of PSLR



(b) Mean value of ISLR

Figure 13: Mean values of the PSLR and ISLR versus SNR for the SFPC, treated with IFFT, and M.SFPC, treated with FD, using polyphase P4 ($M = 100$).

Table 7: Summary of the performance of various waveforms

Waveform	SCPC	SFPC	SFPC	M.SFPC
Algorithm	MF	FD	IFFT	FD
$F_s^{(Rx)}$ (MHz)	B	B/N_p	B/N_p	B/N_p
R_{res}	c/B	c/B	$c/2B$	c/B
No. of pulses	1	N_p	N_p	N_p
R_{min}	$cT_p/2$	$cT_p N_p/2$	$cT_p N_p/2$	$cT_p/2$
PSLR(dB)	-26.32	-13.2	-12	[-21; -29.3]
ISLR(dB)	-13.88	-6.67	-10.4	[-7.8; -13.7]
Artifacts	No	No	Yes	No

4.4. Summary about M.SFPC vs. both SCPC and SFPC

The various waveforms that have been examined in this section are listed in Table. 7. The values of the PSLR and the ISLR are measured for a P4 code in a noiseless environment. This table illustrates how the M.SFPC waveform processed with the FD algorithm outperforms both the SCPC and the SFPC waveforms. From one side, both the SCPC and the M.SFPC waveforms exhibit same range resolution and minimum range. Nevertheless, $F_s^{(Rx)}$ is much smaller in M.SFPC waveform, which is a great advantage. Furthermore, the latter approximately achieves the same PSLR, and even better than that of the SCPC in some situations depending on N_p . From the other side, the comparison between the M.SFPC and the SFPC waveforms processed with the FD algorithm, reveals that both waveforms attain the same range resolution and require the same sampling frequency at the receiver for the same number of transmitted pulses. However, the former leads to better PSLR and ISLR. Moreover, R_{min} is much shorter. If the SFPC is processed with the IFFT algorithm instead, R_{res} is enhanced by a factor of two, and also the ISLR becomes much better. Nonetheless, compared with the M.SFPC waveform, it still achieves higher PSLR and R_{min} . In the same context, one may wonder why we do not exploit the amplitude windowing with the SFPC as an alternative approach to the M.SFPC, knowing that both are processed with the FD algorithm. It is true that amplitude windowing reduces the range sidelobes of the HRRP. However this reduction comes at an increase in the range resolution. To cope with this shortcoming, the M.SFPC is designed to permit a reconstruction of a spectrum at the receiver that is close as much as possible to that of the phase code initially used at the transmitter. In this case, there is no need to apply windowing to the reconstructed spectrum.

4.5. Studying the performance of the M.SFPC waveform in a real radar scenario

In this subsection, our purpose is to study the performance of the M.SFPC waveform in a realistic scenario. Its performance is compared with that of the SFPC waveform processed with the IFFT algorithm. Suppose it is required to detect and identify a certain target from some of its scatterers. In this case, let us consider

four point scatterers with reflection coefficients $[A_1 A_2 A_3 A_4]=[0.5 0.7 0.2 1]$. The ranges between the scatterers and the radar are $[R_1 R_2 R_3 R_4]=[30006m 30009m 30015m 30018m]$.

A Monte-Carlo simulation is carried out for each of the M.SFPC and the SFPC waveforms where a polyphase P4 with $M = 100$ is used. The parameters of the two waveforms are given in Table. 8. In addition, the SNR is equal to 5 dB. It is defined as the ratio between the power of the received pulse that corresponds to the scatterer that has the smallest reflection coefficient and the power of the noise. For a fair comparison, we resort to a scenario where both waveforms have the same instantaneous bandwidth, hence they require the same value of $F_s^{(Rx)}$. Moreover, the total occupied bandwidth B of both waveforms is the same. In addition, $\frac{\Delta F \cdot T_p}{M} = 0.5$ has been taken into consideration for the SFPC waveform. The latter is a necessary condition for the IFFT algorithm to prevent ambiguous returns from folding in a certain region [3]. In Fig. 14 and Fig. 15, the HRRP of the SFPC waveform and the M.SFPC waveform are respectively presented. It turns out that with the SFPC waveform, the third scatterer cannot be discerned from the sidelobes of the other scatterers, as shown in Fig. 14. Moreover, the straddle loss associated with the IFFT algorithm [3] reduces the apparent amplitude of the second scatterer as shown in Fig. 14. In contrast, with the M.SFPC waveform, the same scatterer can easily be identified, as shown in Fig. 15. This result clearly reveals the advantage of the better PSLR of the M.SFPC waveform. Furthermore, the SFPC waveform requires longer CPI for the burst of pulses ($N_p = 13$) to be transmitted, and the value of its minimum range ($R_{min} = 600$ m) is four times larger than that of the M.SFPC waveform. Nevertheless, it attains a range resolution $R_{res} = 0.75m$ which is twice better than that of the M.SFPC waveform.

Table 8: Parameters for comparing the M.SFPC and the SFPC waveforms using the IFFT algorithm. Polyphase P4 is used as an intra-pulse modulation

Parameter	M.SFPC	SFPC
N_p (μs)	4	13
f_c (GHz)	9.2	9.2
PRF (Hz)	2300	2300
T_p (μs)	1	4
B_{inst} (MHz)	25	25
$F_s^{(Rx)}$ (MHz)	50	50
Δf (MHz)	50	12.5
B (MHz)	200	200
B_{eff} (MHz)	100	200

5. Conclusions and perspectives

In this paper, the relevance of the simple yet efficient FD algorithm to treat the echoes of the SFPC waveform is studied. Our investigations have revealed that treating

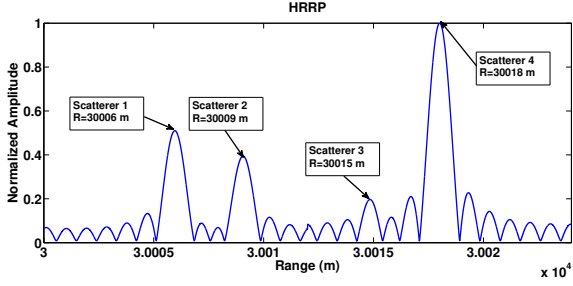


Figure 14: The HRRP of the SFPC waveform processed with the IFFT algorithm.

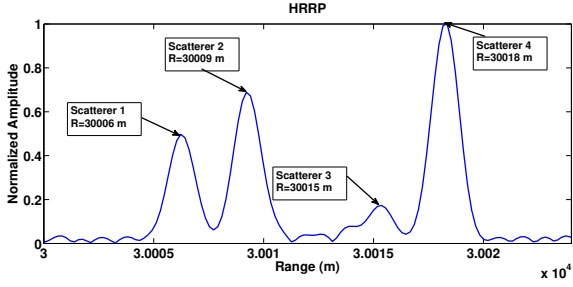


Figure 15: The HRRP of the M.SFPC waveform.

the latter waveform with either the FD algorithm or the IFFT algorithm could not exploit the PSLR and the ISLR that result from the autocorrelation function of the phase code used. Hence, to overcome this shortcoming, we have proposed a modified SFPC radar waveform. Contrasting this waveform with the SCPC waveform reveals that the M.SFPC waveform makes it possible to attain and even exceed the PSLR and the ISLR of such phase codes in the overlapping scenarios. This is achieved while still making use of the existing FD algorithm with some minor modifications to treat the received echoes. Moreover, contrasting the M.SFPC waveform with the SFPC waveform reveals that the former outperforms the latter in terms of PSLR, ISLR, and R_{min} . To sum up, the M.SFPC waveform is suitable for applications that seek a high range resolution, small minimum range and a low computational cost. We believe that our proposed approach is not restricted to the SFPC scheme, but could rather be used with other SF schemes like SF-NLFM. Finally, in the future, we are going to investigate these schemes, following the same methodology that has been applied with the SFPC waveform in this paper.

6. Acknowledgements

This project has been funded with support from the National Council for Scientific Research in Lebanon.

7. Appendices

Appendix A

Applying an IDFT to (13), yields:

$$z_r(n) = \frac{1}{(2N-1)N_p} \times \sum_{l_1=0}^{(2N-1)N_p-1} Z_{r,total}(l_1+1) \exp\left[\frac{j2\pi l_1 n}{(2N-1)N_p}\right] \quad (\text{A.1})$$

where $Z_{r,total}(l)$ is the l^{th} element of $Z_{r,total}$. Using (4), the above equation can be expressed as follows:

$$z_r(n) = \frac{\exp\left[-j2\pi\left(f_c + \left[\frac{1-N_p}{2}\right]\Delta f\right)\frac{2R}{c}\right]}{(2N-1)N_p} \sum_{l=0}^{N_p-1} \exp\left[-j2\pi l\left(\Delta f\frac{2R}{c} - \frac{n}{N_p}\right)\right] \sum_{k=0}^{2N-2} \exp\left[-j\frac{2\pi k}{(2N-1)}\left(\frac{2RF_s^{(R_x)}}{c} - \frac{n}{N_p}\right)\right] \quad (\text{A.2})$$

Therefore, its modulus is equal to:

$$|z_r(n)| = \frac{1}{(2N-1)N_p} \frac{|\sin\left[N_p\pi\left(\Delta f\frac{2R}{c} - \frac{n}{N_p}\right)\right]|}{|\sin\left[\pi\left(\Delta f\frac{2R}{c} - \frac{n}{N_p}\right)\right]|} \frac{|\sin\left[\pi\left(\frac{2RF_s^{(R_x)}}{c} - \frac{n}{N_p}\right)\right]|}{|\sin\left[\frac{\pi}{2N-1}\left(\frac{2RF_s^{(R_x)}}{c} - \frac{n}{N_p}\right)\right]|} \quad (\text{A.3})$$

$$\text{If } n = \frac{2RF_s^{(R_x)}N_p}{c}, \frac{|\sin\left[\pi\left(\frac{2RF_s^{(R_x)}}{c} - \frac{n}{N_p}\right)\right]|}{|\sin\left[\frac{\pi}{2N-1}\left(\frac{2RF_s^{(R_x)}}{c} - \frac{n}{N_p}\right)\right]|} = 2N-1.$$

$$\text{Moreover, if } F_s^{(R_x)} = \Delta f, \frac{|\sin\left[N_p\pi\left(\Delta f\frac{2R}{c} - \frac{n}{N_p}\right)\right]|}{|\sin\left[\pi\left(\Delta f\frac{2R}{c} - \frac{n}{N_p}\right)\right]|} = N_p \text{ and}$$

$$|z_r(n)| = 1$$

Appendix B

The relation between the discrete-time Fourier Transform (DTFT) of the sequence $p_{ref,l}(n)$ and that of its down-sampled version $p_{ref,l}^{down}(n)$ is given by:

$$P_{ref,l}^{down}(f) = \frac{1}{N_p} \sum_{m=0}^{N_p-1} P_{ref,l}\left(f - m\frac{F_s^{(Tx)}}{N_p}\right) \quad (\text{B.1})$$

This amounts to reproducing N_p times $P_{ref}(f)$, or equivalently a portion of the Fourier transform $V(f)$, with a shift of frequency equal to $k\frac{F_s^{(Tx)}}{N_p}$ with $k = 1, \dots, N_p - 1$. Since the latter is band-limited on a frequency band equal to $\frac{F_s^{(Tx)}}{N_p}$, the different terms of the sum in (B.1) do not overlap. Hence, by taking advantage of the periodicity of the DTFT, (B.1) in the frequency band $[0, \frac{F_s^{(Tx)}}{N_p}]$ reduces

to:

$$P_{ref,l}^{down}(f) = \begin{cases} \frac{1}{N_p} P_{ref,l}(f) & \text{if } f \in [0, \frac{F_s^{(Tx)}}{2N_p}] \\ \frac{1}{N_p} P_{ref,l}(f + (N_p - 1)\frac{F_s^{(Tx)}}{N_p}) & \text{if } f \in [\frac{F_s^{(Tx)}}{2N_p}, \frac{F_s^{(Tx)}}{N_p}] \end{cases} \quad (\text{B.2})$$

Given (B.2), a relation can be deduced between the DFT of $\{p_{ref,l}(n)\}_{n=0,\dots,N-1}$ and that of $\{p_{ref,l}^{down}(n)\}_{n=0,\dots,N/N_p-1}$ computed at the sampling frequency $F_s^{(Tx)}$ and $\frac{F_s^{(Tx)}}{N_p}$ respectively. This can be written for the k^{th} frequency bin as follows:

$$P_{ref,l}^{down}(k) = \begin{cases} \frac{1}{N_p} P_{ref,l}(k) & \text{if } k \in \llbracket 0, \frac{N}{2N_p} - 1 \rrbracket \\ \frac{1}{N_p} P_{ref,l}(k + (N_p - 1)\frac{N}{N_p}) & \text{if } k \in \llbracket \frac{N}{2N_p}, \frac{N}{N_p} - 1 \rrbracket \end{cases} \quad (\text{B.3})$$

Appendix C

In the following, $x_L(n)$ denotes the original signal with length L and $x_M(n)$ is the original signal padded with zeros whose length is M . Given $X_L(k)$ the DFT of $x_L(n)$, θ the normalized angular frequency with respect to the sampling frequency, and k the frequency bin, let us recall the DTFT and the IDFT of $X_L(k)$:

$$X_L(\theta) = \sum_{n=0}^{L-1} x_L(n) \exp(-jn\theta) \quad (\text{C.1})$$

and

$$x_L(n) = \frac{1}{L} \sum_{k_1=0}^{L-1} X_L(k_1) \exp\left(j\frac{2\pi k_1 n}{L}\right) \quad (\text{C.2})$$

By substituting (C.2) in (C.1), the latter becomes:

$$\begin{aligned} X_L(\theta) &= \sum_{n=0}^{L-1} \frac{1}{L} \sum_{k_1=0}^{L-1} X_L(k_1) \exp\left(j\frac{2\pi k_1 n}{L}\right) \cdot \exp(-jn\theta) \\ &= \sum_{k_1=0}^{L-1} X_L(k_1) \cdot \frac{1}{L} \sum_{n=0}^{L-1} \exp\left(j\left(\frac{2\pi k_1}{L} - \theta\right)n\right) \\ &= \sum_{k=0}^{L-1} X_L(k) \cdot \exp\left(-j\left(\frac{\theta}{2} - \frac{\pi k_1}{L}\right)(L-1)\right) \quad (\text{C.3}) \\ &\quad \cdot \text{psinc}_L\left(\theta - \frac{2\pi k_1}{L}\right) \end{aligned}$$

where

$$\text{psinc}_L(\theta) = \frac{1}{L} \frac{\sin(\frac{L\theta}{2})}{\sin(\frac{\theta}{2})} \quad (\text{C.4})$$

The latter is equal to 1 if $\theta = 0$ and to 0 if θ is a multiple of $\frac{2\pi}{L}$. Otherwise, intermediate values are obtained. The DFT of the padded signal $x_M(n)$ is given by evaluating $X_L(\theta)$ at the normalized angular frequency $\theta = k\frac{2\pi}{M}$ where

$k \in \llbracket 0, M-1 \rrbracket$. Hence, $X_M(k)$ is given by:

$$\begin{aligned} X_M(k) &= \sum_{k_1=0}^{L-1} X_L(k_1) \exp\left(-j\pi\left(\frac{k}{M} - \frac{k_1}{L}\right)(L-1)\right) \\ &\quad \cdot \text{psinc}_L\left(2\pi\left(\frac{k}{M} - \frac{k_1}{L}\right)\right) \end{aligned} \quad (\text{C.5})$$

No simplification or approximation can be really done at this stage. All the values of the DFT of the non-padded signal contribute to get the values of the DFT of the padded signal. They are weighted by $\text{psinc}_L\left(2\pi\left(\frac{k}{M} - \frac{k_1}{L}\right)\right)$. It should be noted that for a given k , the values of k_1 that lie in the main lobe of the psinc function satisfies: $k\frac{L}{M} - 1 < k_1 < k\frac{L}{M} + 1$. When $M = 2L - 1$, $k\frac{L}{2L-1} - 1 < k_1 < k\frac{L}{2L-1} + 1$. If the above approach is applied to the sequence $p_{ref}^{down}(n)$ with $L = \frac{N}{N_p}$ and $M = \frac{2N}{N_p} - 1 = 2L - 1$, this leads to:

$$\begin{aligned} P_{ref,l}^{dopad}(k) &= \sum_{k_1=0}^{\frac{N}{N_p}-1} P_{ref,l}^{down}(k_1) \\ &\quad \cdot \exp\left(-j\pi\left(\frac{k}{2N-N_p} - \frac{k_1}{N}\right)(N-N_p)\right) \\ &\quad \cdot \text{psinc}_{\frac{N}{N_p}}\left(2\pi N_p\left(\frac{k}{2N-N_p} - \frac{k_1}{N}\right)\right) \end{aligned} \quad (\text{C.6})$$

References

- [1] R. T. Lord, Aspects of stepped-frequency processing for low-frequency SAR systems, PhD thesis, University of Cape Town, Dept of Electrical Engineering, 2000.
- [2] D. R. Wehner, High resolution radar, Artech House, London, UK, 1995.
- [3] W. L. Melvin, J. A. Scheer, Principles of modern radar, Vol. II: Advanced techniques, SciTech Publishing, 2013.
- [4] W. Zhai, Y. Zhang, Application of super-SVA to stepped-chirp radar imaging with frequency band gaps between subchirps, Progress in electromagnetics research B 30 (2011) 71–82.
- [5] H. Yuan, S. Wen, Z. Cheng, Study on I SAR imaging of stepped-frequency chirp signal, Proceedings of the 26th Conference of Spacecraft TT&C Technology 187 (2012) 197–210.
- [6] M. Y. Chua, V. C. Koo, H. S. Lim, J. T. S. Somantyo, Phase coded stepped frequency linear frequency modulated waveform synthesis technique for low altitude ultra wideband synthetic aperture radar, IEEE Access 5 (2017) 11391–11403.
- [7] R. Liu, Y. Wang, Imaging approach for airborne stepped-frequency synthetic aperture radar in the squinted mode, Journal of applied remote sensing 11 (1) (2017) 1–15.
- [8] X. Luo, Y. Deng, R. Wang, W. Guo, Imaging for MIMO sliding spotlight SAR using stepped frequency chirps, EUSAR, 10th European Conference on Synthetic Aperture Radar (2014).
- [9] Y. Luo, Q. Zhang, C. W. Qiu, X. J. Liang, K. M. Li, Micro-Doppler effect analysis and feature extraction in ISAR imaging with stepped-frequency chirp signals, IEEE Transactions on Geoscience and Remote Sensing 48 (4) (2010) 2087–2098.
- [10] T. Li, H. Yang, Z. Zhou, RFI suppression based on phase-coded stepped-frequency waveform in through-wall radars, IEEE Transactions on Geoscience and Remote Sensing 53 (2015) 1583–1591.
- [11] C. Fukushima, N. Hamada, A study on stepped frequency radar by using intra-pulse phase coded modulation, Proceedings of the World Congress on Engineering and Computer Science (2008).
- [12] I. Gladkova, D. Chebanov, Grating lobes suppression in stepped-frequency pulse train, IEEE Transactions on Aerospace and Electronic Systems 44 (2008) 1265 – 1275.

- [13] R. T. Lord, M. R. Inggs, High resolution SAR processing using stepped frequencies, IEEE, Geoscience and Remote Sensing, IGARSS (1997) .
- [14] E. L. Key, E. N. Fowle, R. D. Haggarty, A method of side-lobe suppression in phase-coded pulse compression systems, Technical report, M.I.T Lincoln Laboratory (209) (1959) .
- [15] M. H. Ackroyd, F. Ghani, Optimum mismatched filters for side-lobe suppression, IEEE Transactions on Aerospace and Electronic Systems 9 (2) (1973) 214 – 218.
- [16] A. J. Wilkinson, R. T. Lord, M. R. Inggs, Stepped-frequency processing by reconstruction of target reflectivity spectrum, Proceedings of the South African Symposium on Communications and Signal Processing (1998) .
- [17] W. G. Carrara, R. S. Goodman, , R. M. Majewski, Spotlight synthetic aperture radar: signal processing algorithms, Artech House, 1995.
- [18] G. Lellouch, A. K. Michra, M. Inggs, Design of OFDM radar pulses using genetic algorithm based techniques, IEEE Transactions on Aerospace and Electronic Systems 52 (4) (2016) 1953–1966.
- [19] Z. Ge, P. Huang, W. Lu, Matched NLFM pulse compression method with ultra-low sidelobes, In Proceedings of the 5th European Radar Conference (2008) 92–95.
- [20] G. Galati, G. Pavan, F. DePalo, Chirp signals and noisy waveforms for solid-state surveillance radars, MDPI Aerospace 4 (2) (2017) .
- [21] S. Alphonse, G. A. Williamson, Novel radar signal models using nonlinear frequency modulation, Proceedings of the 22nd European Signal Processing Conference (EUSIPCO) (2014) 1024–1028.
- [22] X. He, N. Tong, X. Hu, High-resolution imaging and 3-D reconstruction of precession targets by exploiting sparse apertures, IEEE Transactions on Aerospace and Electronic Systems 53 (3) (2017) 1212 – 1220.
- [23] X. He, N. Tong, X. Hu, Dynamic ISAR imaging of maneuvering targets based on sparse matrix recovery, Elsevier Signal Processing 134 (2017) 123 – 129.
- [24] S.-M. Omar, F. Kassem, R. Mitri, M. Saleh, H. Hijazi, A novel barker code algorithm for resolving range ambiguity in high PRF radars, Proceedings of the 12th European Radar Conference (EuRAD) (2015) .